Room-Temperature Generation of Heralded Single Photons on Silicon Chip with Switchable Orbital Angular Momentum

Shan Zhang, Xue Feng,* Wei Zhang, Kaiyu Cui, Fang Liu, and Yidong Huang

In quantum optics, orbital angular momentum (OAM) is very promising to achieve high-dimensional quantum states due to the nature of infinite and discrete eigenvalues, which is quantized by the topological charge of l. Here, a heralded single-photon source with switchable OAM modes is proposed and demonstrated on silicon chip. At room temperature, the heralded single photons with 11 OAM modes ($l = 2–6$, $−6$ to $−1$) are successfully generated and switched through thermo-optical effect. It is believed that such an integrated quantum source with multiple OAM modes and operating at room temperature can provide a practical platform for high-dimensional quantum information processing. Moreover, this proposed architecture can also be extended to other material systems to further improve the performance of OAM quantum source.

1. Introduction

The orbital angular momentum (OAM) is an independent degree of freedom of photons, which corresponds to the spiral phase fronts, with the quantized eigenvalue as the topological charge (l).[1] Benefiting from the unique characteristics of the infinite and discrete topological charges, OAM modes are natural for generating high-dimensional states and could increase the information capacity carried by photons.[2–5] Especially in quantum domain, it is strongly desired to increase the information content encoded on a single photon for higher efficiency, better noise resistance, richer resources, and more flexibility of quantum communications, computations, and simulations.[6–9] So far, OAM encoded quantum states have been utilized in quantum key distribution,[10–13] quantum ghost imaging,[14,15] and high-dimensional quantum entanglement.[16,17] The potential application of high-dimensional quantum information has stimulated the research on generating,[18,19] manipulating,[20,21] and detecting[22,23] the optical quantum states encoded with OAM modes.

As an effective way to achieve higher dimensional quantum states, OAM single-photon sources are mainly demonstrated via the spontaneous parametric down-conversion in nonlinear crystals,[24–27] where bulky spatial optical systems are required. Clearly, an integrated OAM quantum source is preferred for its compactness, high stability, and flexibility. The pioneer work of the integrated OAM single-photon source is demonstrated with InAs/GaAs epitaxial quantum dots embedded in a microring cavity, in which the OAM modes with $|l| = 6$ have been successfully generated at 30 K.[28] To utilize the high-dimensional feature, the usable OAM modes should be as more as possible after considering both applications of multiplexing and dynamic coding,[17] and the latter also requires that the topological charges could be dy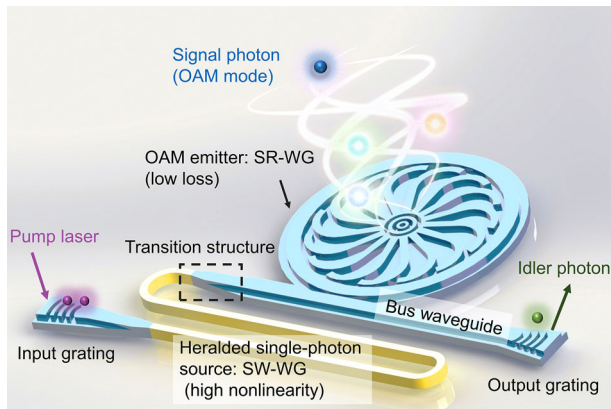namically switched. We have recently demonstrated a heralded single-photon source with switchable OAM modes, in which five OAM modes ($l = 3–7$) can be obtained with fixed incident wavelength.[29] However, such work is based on the spontaneous four-wave mixing (SFWM) in dispersion-shifted fiber (DSF) so that it is not a fully on-chip device and cooling to 77 K is still required to reduce the Raman scattering noise in DSF.[30] Till now, an integrated quantum light source with switchable OAM modes and operating at room-temperature has not yet been realized.

To tackle the aforementioned two challenges, we have proposed and demonstrated an integrated heralded single-photon source with 11 switchable OAM modes operating at room-temperature in this work. The whole device is integrated on a monolithic silicon chip and spatially divided into two parts: generating correlated photon pairs and then transforming to OAM modes. Here, the heralded single-photon source is based on the SFWM in a silicon wire waveguide (SW-WG) as a result of its high nonlinearity and narrow Raman bandwidth.[31–33] The noises caused by Raman scattering could be filtered without the cryogenic requirement so that the whole device could operate at room temperature. For mode transformation, an integrated OAM emitter based on the shallow ridge waveguide (SR-WG) could load the OAM modes onto single photons.[34] Benefitting from the spatial separation of the source and emitter, the room-temperature operating condition, and the high thermo-optical coefficient of silicon, the topological charges of generated OAM modes can be switched through the thermo-optical effect[35] while the performance of single-photon emission is not disturbed. Assembling both the heralded single-photon source and OAM emitter by a well-designed transition structure, the heralded single photons with switchable OAM modes ($l = 2–6$, $−6$ to $−1$) are obtained. The coincidence counts (CCs) and coincidence counts-to-accidental coincidence counts ratio (CAR) are

S. Zhang, X. Feng, W. Zhang, K. Cui, F. Liu, Y. Huang
Department of Electronic Engineering
Tsinghua University
Beijing 100084, China
E-mail: x-feng@tsinghua.edu.cn

DOI: 10.1002/lpor.202200388

**ADVANCED
SCIENCE NEWS**

www.advancedsciencenews.com

LASER
& PHOTONICS
REVIEWS

www.lpr-journal.org

Figure 1. The schematic of integrated heralded single-photon source with switchable OAM modes. SW-WG: silicon wire waveguide; SR-WG: shallow ridge waveguide. Such two types of waveguides are utilized due to the features of the low transmission loss and high nonlinearity, respectively. The device is based on the silicon platform and the different colors are used to distinguish different waveguides (SW-WG and SR-WG).

measured as 27.5–82 and 16.33–57.63 within 10 min for 11 OAM modes, respectively. It should be mentioned that there is no obvious deterioration of the CAR value compared with that of SW-WG alone (34.09–52.05). Thus, the correlation between photon pairs is kept after the mode conversion of OAM emitter. We believe that this work is essential for exploring the application of OAM modes in high-dimensional quantum information processing.

2. Results

2.1. Principle

The whole device is fabricated on the silicon platform for both high nonlinearity and thermo-optical coefficient. The silicon-on-insulator substrate with top silicon thickness of 220 nm is utilized here. As shown in **Figure 1**, to generate the single-photon state with switchable OAM modes on chip, our proposal is to utilize the spatially separated single-photon source and OAM emitter. With proper structural design, a heralded single-photon source could be realized through degenerate SFWM in SW-WG (yellow section in Figure 1), where correlated photon pairs are generated at room temperature.[31,32,36] Each photon pair can be divided into signal and idler photon according to their wavelengths. Through the wavelength-selecting feature of microring cavity in the OAM emitter, the signal photon would be coupled into the emitter and converted to OAM modes, while the idler photon is scattered from the output grating directly. Thanks to the room-temperature operation of heralded single-photon source as well as the spatial separation of the source and emitter, a thermo-optical controller attached to OAM emitter can be utilized to switch the topological charges of generated OAM modes. Finally, the CCs and CAR between signal and idler photon could confirm the successful generation of the heralded single photons with switchable OAM modes. **Figure 2**a is the microphotograph of the fabricated device and the pump laser is coupled into SW-WG through the vertical input grating (shown as the inset in left bottom of Figure 2a).

For most quantum light sources based on nonlinear processes, Raman scattering noise is the main factor deteriorating the signal-to-noise ratio (SNR). It is worth mentioning that, due to the crystal nature of silicon material, the linewidth of Raman scattering is as narrow as 103 GHz and located 15.6 THz away from the pump frequency.[31] Thus, the Raman noise could be readily filtered out at room temperature. In order to obtain a higher nonlinear coefficient, the width and height of the SW-WG are designed as 460 nm × 220 nm[32] whose cross-profile is shown in Figure 2b. Moreover, the length of SW-WG is considered as the trade-off between the correlated photon-pair generation rate and transmission loss. After some experimental measurements, the length is set as 5 mm (see Figure S1 in Supporting Information). For generated photon pairs, we take the signal photon as heralded single photon and idler photon as heralding single photon in this work. Actually, the heralded single photon is post-selected by CCs between these two photons. Meanwhile, the calculated CAR can evaluate the SNR of the heralded single-photon source.[37–39]

The design of OAM emitter is based on our previous work.[34] It consists of a bus waveguide, microring cavity, 32 azimuthally uniformly distributed download waveguides, and scattering grating in the center of the cavity. The download waveguides would pick up part of the whispering gallery mode (WGM) around the microring cavity and collect them to the scattering grating (Figure 2d). Conditioned on the intrinsic angular momentum of WGM, the scattered mode would carry the OAM. When the number of download waveguides is fixed, the topological charges of generated OAM modes directly depend on the order of WGM (details are shown in Supporting Information). Thus, we can vary the order of WGM with thermo-optical controller (titanium electrode above microring cavity), in turn switching the topological charges at fixed incident wavelength. To improve the efficiency of thermo-optical controller, the radius of microring cavity is designed as 200 μm for a narrower free spectral range (FSR) nearly to 0.5 nm. As shown in Figure 2c, for a lower transmission loss, the SR-WG is utilized for the OAM emitter. The etching depth and width of SR-WG are 70 nm and 1 μm, respectively. Obviously, there are two types of waveguides corresponding to the heralded single-photon source and OAM emitter, respectively. Hence, a transition structure is designed between them so that the SW-WG is gradually transformed to SR-WG within a length of 100 μm.[40] Figure 2e shows the gradually enlarged SR-WG in transition structure. It should be mentioned that the thermo-optical controller is also important for precisely tuning the operating wavelength of the OAM emitter according to the wavelength of signal photons. By properly setting the wavelengths of the pump and signal/idler photons, together with the thermo-optical controller, the signal photons can be coupled into the OAM emitter and converted to OAM modes while the pump and idler photons are not. It should be mentioned that only the pure OAM states can be generated and switched with the OAM emitter in this work. Actually, the OAM modes can also be employed to achieve superimposed quantum states. In our previous work,[41] an integrated OAM emitter has been proposed and demonstrated to generate optical superimposed vortex beam with tunable OAM. Thus, with such OAM emitter and a quantum source, which is similar to the heterogenous structure shown in Figure 1, quantum states with multiple OAM modes could also be obtained.
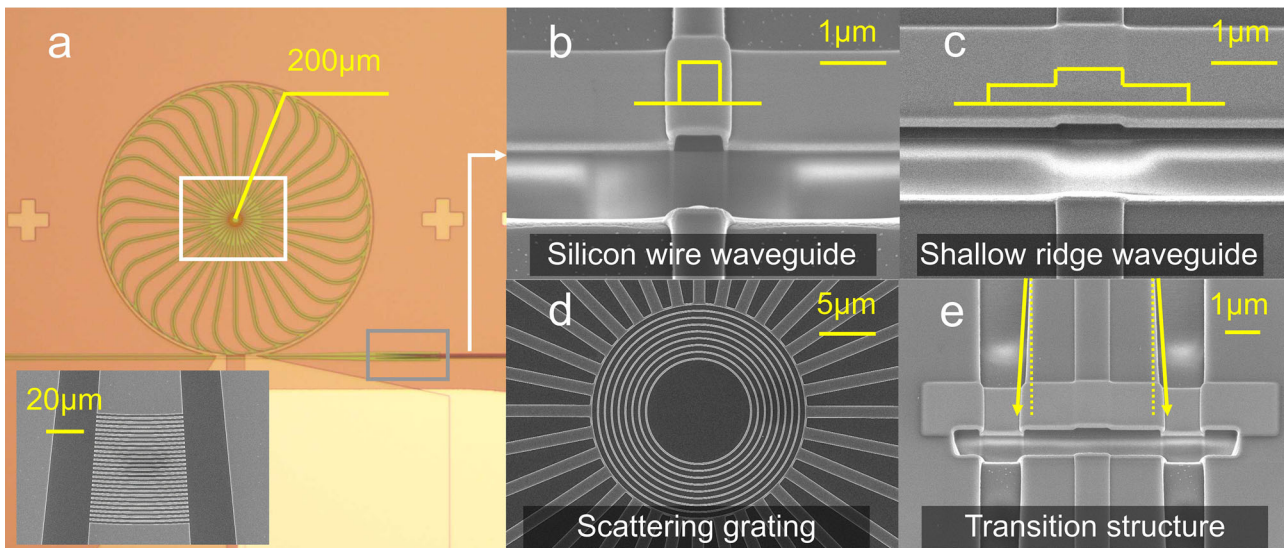
Figure 2. Photographs of the fabricated device. a) The microphotograph of the whole device and the inset is the scanning electron microscope (SEM) photograph of the input grating (same as output grating). b) The SEM photograph of silicon wire waveguide, c) shallow ridge waveguide, d) scattering grating (marked by white box in (a)), and e) transition structure (marked by gray box in (a)). The period and duty cycle of scattering grating are 630 nm and 50%, same as the input (output) grating. The platinum is deposited above the waveguide to protect its morphology as shown in (b), (c), and (e).
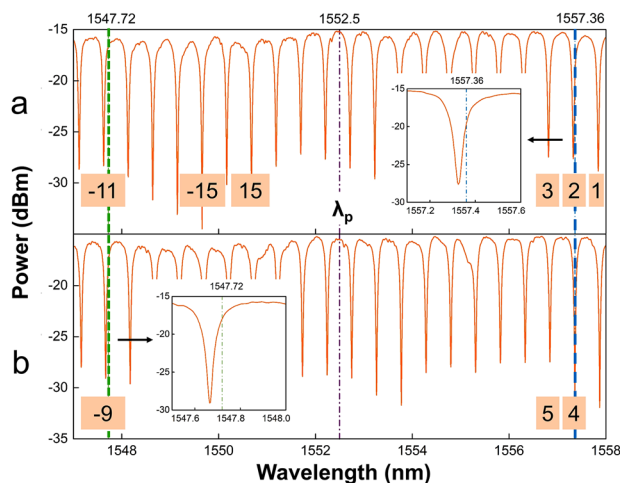

Figure 3. The transmission spectrum of the OAM emitter with driving voltage of a) 0 V and b) 13.97 V. The insets are the zoom-in figures for more clarity. Some typical topological charges corresponding to the resonant wavelength near λ_s and λ_i are marked in orange boxes.

2.2. The Characteristics of OAM Emitter

To determine the arrangement of pump, signal, and idler wavelengths, the transmission spectrum of the OAM emitter is measured at the beginning. A tunable laser is coupled into the emitter through the input grating while the laser power is set as 0 dBm to alleviate the nonlinear loss in SW-WG. Meanwhile, the driving voltage of thermo-optical controller is set as 0 V and the intrinsic transmission spectrum of the emitter could be obtained by scanning the resonant wavelength of the OAM emitter. As shown in **Figure 3**a, the FSR and full-width half-maximum (FWHM) are ≈0.5 and ≈0.045 nm, respectively. The corresponding relation

between the resonant wavelength and topological charge could be identified through the interference patterns of the generated OAM modes and Gaussian mode[42] (see Figure S2 in Supporting Information). There are some typical topological charges marked below the corresponding resonant wavelength. To avoid the non-linear process in microring cavity, which would introduce unexpected noises, the pump photons should directly propagate through the bus waveguide and be scattered from the output grating as well as the idler photons. Thus, after considering both resonant wavelengths and the group velocity dispersion of SW-WG, the wavelength of pump laser (λ_p) is set as 1552.5 nm. Moreover, the signal wavelength has to be aligned with the resonant wavelength of microring cavity while the idler wavelength does not and both of them should follow the relation for SFWM as $\omega_s + \omega_i = 2\omega_p$ (ω_s, ω_i, and ω_p are angular frequencies of signal, idler, and pump photons). As shown in Figure 3, for OAM mode with $l = -6$ to -1, the signal wavelength (λ_s) is set as 1547.72 nm (marked as green dashed line in Figure 3) while correspondingly, the idler wavelength (λ_i) is 1557.36 nm (marked as blue line in Figure 3). For OAM modes of $l = 2-6$, λ_s and λ_i are exchanged, since the resonant wavelength of $l = 2$ is closer to 1557.36 nm (more discussion are shown in Supporting Information). Moreover, the spectrum would be red-shifted as increasing the driving voltage so that an arbitrary resonant wavelength could always be aligned with the fixed signal wavelength. As an example, the spectrum as driving voltage equals 13.97 V is shown in Figure 3b, in which the OAM mode of $l = 4$ is aligned with λ_s while correspondingly, λ_i is misaligned with the resonant wavelength. In this work, limited by maximum driving voltage, 11 OAM modes correspond to two signal wavelengths (1547.72 or 1557.36 nm). Actually, all OAM modes could be achieved at a fixed signal wavelength by increasing the driving voltage.

The emission efficiency and mode purity of OAM emitter are also evaluated with the tunable laser. Here, the incident
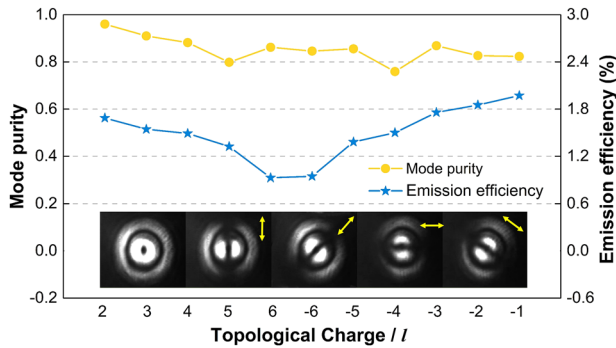
Figure 4. The mode purities and emission efficiencies of 11 OAM modes. The insets are the intensity cross-sections of the generated OAM mode with $l = 0$ before (the first one) and after a polarizer. The directions of the polarization for the latter four insets are marked by yellow arrows.

wavelength is same as λ_s. Specifically, OAM modes with $l = -6$ to -1 and $l = 2$–6 are measured at the incident wavelength of 1547.72 and 1557.36 nm, respectively. With a fixed incident wavelength, the topological charges could be switched by varying the driving voltage on thermo-optical controller. The emission efficiency is defined as $\frac{P_{out}}{P_{in}}$. Here, P_{in} is the optical power coupled into the OAM emitter, which can be calculated as the input power subtracting the vertical coupling loss and the insertion loss of the SW-WG. P_{out} is the optical power collected directly above the emitter. According to our experiments, the losses of vertical coupling and SW-WG are estimated as 7 and 1 dB, respectively. Then, the emission efficiencies versus varied topological charges are shown as the blue stars in **Figure 4**. Moreover, the mode purity of the generated OAM mode with topological charge of l is defined as $\frac{P_l}{\sum_{m=-6}^{6} P_m}$, in which P_x ($x = l/m$) is the power of the OAM mode with topological charge of l or m. Here, the topological charge range of $m = -6$ to 6 is considered as the bases. It should be mentioned that the generated OAM modes are azimuthally polarized, which is a kind of vectorial polarized beam and can be seen in the insets of Figure 4.[43] The doughnut intensity profile in first column corresponds to the OAM mode with $l = 0$ and the other four images are the intensity cross-sections after passing through a polarizer with different directions as marked by the yellow arrows. More results about measured polarization states for $l = 2$–6 and $l = -6$ to -1 could be found in the Supporting Information (Figure S2, Supporting Information). With the utilized OAM emitter, the polarization of generated OAM modes would always be azimuthal and keep constant with varied driving voltage. Actually, the polarization state depends on the coupling structure to extract the WGM mode. In the microring cavity, the fundamental mode is the quasi-transverse electric (TE) WGM, thus if download waveguides or scattering units are distributed on the sidewall of the cavity waveguide, azimuthally polarized OAM modes can be generated, which is the case of this work. When the scattering units are distributed on the top of the cavity waveguide, the generated OAM modes are radially polarized, which can be found in our previous work.[44] The azimuthal polarization could be equally decomposed to left-handed and right-handed circularly polarized (LHCP and RHCP) components with the topological charge donated as l_L and l_R. They satisfy the relation of $l = l_L - 1 = l_R + 1$.[34] Since the topological charge of l_L

and l_R is different, the azimuthally polarized OAM modes generated from the emitter should be first decomposed to LHCP and RHCP components to measure the mode purities. With spatial light modulator (SLM) serving as a mode filter, a certain OAM mode would be extracted according to the helical phase masks on SLM. Since the SLM operates in linearly polarized incidence, the LHCP or RHCP component has to be transformed to linear polarization before the SLM. In each measurement of LHCP or RHCP component, the topological charge of the phase mask on SLM (l_{mask}) would be switched within the range of $l_{mask} = -7$ to 7 to extract the corresponding modes and 15 values of optical power could be obtained. The mode purity is calculated as the power ratio of the considered OAM mode over the sum of all 15 values (details are shown in the Supporting Information). Here, the values of mode purity have been averaged with the measured values of both LHCP and RHCP components and shown as yellow dots in Figure 4 (the specific results of LHCP and RHCP components are shown in Figure S5 in the Supporting Information).

Theoretically, a higher mode purity could be guaranteed if the power extracted by each download waveguide is as equal as possible. Hence, there is a trade-off between the emission efficiency and mode purity. In this work, the mode purity is taken more concern than the emission efficiency so that the coupling efficiency of each download waveguide is set as low as 1%. Correspondingly, the values of emission efficiency are ranging between 0.93% and 1.97%. It should be noticed that the emission efficiencies would decrease with the increasing absolute values of topological charge. According to the Nyquist theory, the spatial sampling rate would be low for OAM modes with high $|l|$ due to the fixed number of download waveguides, which would introduce a lower emission efficiency. The small fluctuations in measured values may be related to the deviation of chip fabrication. For mode purity, most of the measured values are larger than 80% as shown in Figure 4. Actually, the mode purity is quite critical to the performance of the quantum source, e.g., the indistinguishability of signal–idler photon pairs. With our proposal, the indistinguishability is determined by both the heralded single-photon source based on SW-WG and the OAM emitter. It has been demonstrated that good indistinguishability of heralded single-photon source can be achieved with the SW-WG.[45,46] Thus, high mode purity of the OAM emitter could ensure the indistinguishability as close as possible to that of the heralded single-photon source.

2.3. The Coincidence Counts of Silicon Wire Waveguide

At first, the performance of the SW-WG serving as the heralded single-photon source is evaluated. As shown in Figure 3a, without driving voltage, all of the pump, signal, and idler photons are not coupled into the OAM emitter so that the CCs of the SW-WG could be measured from the output grating. Here, the pump is a pulsed laser (40 MHz, 1552.5 nm), coupled into the SW-WG from the input grating, and then the correlated photon pairs are generated through SFWM process. Afterward, such photon pairs would directly propagate through the bus waveguide and be scattered out of the chip from the output grating. With the help of vertical coupling, the photon pairs are coupled into a fiber-based dense wavelength division multiplexer (DWDM). Thus, the signal and idler photons are separately guided into two single
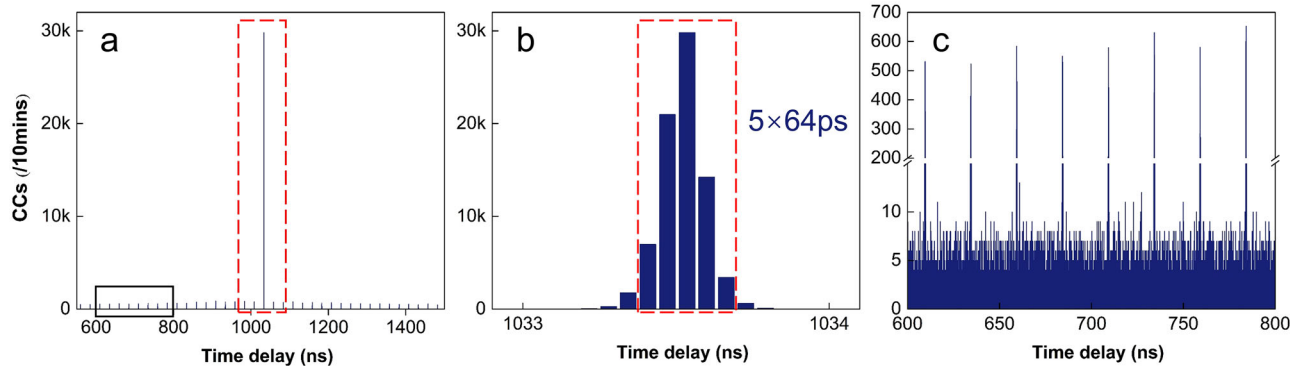
Figure 5. The coincidence counts (CCs) of silicon wire waveguide. a) A typical result of CCs. b) The zoomed-in view of main peak corresponding to the red dashed box in (a). c) The zoomed-in view of side peaks with the time delay of 600–800 ns corresponding to the black box in (a).

photon avalanche diodes (SPADs) connected by time-correlated single photon counting (TCSPC) for CCs measurement. The typical CCs of SW-WG within 10 min are shown in **Figure 5**a, there is a main peak of CCs and some equidistantly distributed small side peaks, which can be clearly observed in the enlarged figures as Figure 5b,c, respectively. In Figure 5b, the main peak is actually broadened due to the time jitter of SPADs.[47] Thus, the CCs are calculated as the sum of the five peaks within a time slot of 320 ps (the red dashed box in Figure 5b) and the result is 77.9 K counts per 10 min. Different from the background noises caused by the dark counts of SPADs, the time interval of the small side peaks corresponds to the period of pulsed laser (25 ns) as shown in Figure 5c.[48] For a heralded single-photon source, CAR is defined as the ratio of CCs to accidental coincidence counts (ACCs). Here, the ACCs are estimated as the value of 14 side peaks evenly distributed around the main peak while the time jitter is also considered. As a result, 14 values of CAR are obtained and the maximum and minimum are 52.05 and 34.09, respectively.

Furthermore, the second-order correlation $g^2(\tau)$ of this heralded single-photon source is measured through the Hanbury-Brown and Twiss interferometer. Specifically, the signal photons are equally divided to two SPADs (SPAD1 and SPAD2), while the time delay between them is τ. The idler photons correspond to the third SPAD (SPAD3). The $g^2(0)$ can be calculated[49,50] by $\frac{C_{123}N_3 t}{C_{13}C_{23}}$, in which C_{123} is threefold CCs of all three SPADs and C_{13}/C_{23} is twofold CCs between SPAD1/SPAD2 and SPAD3, while N_3 and t are the counting rate of idler photons and testing time, respectively. Theoretically, for single-photon source, $0 \leq g^2(0) < 1$ and lower $g^2(0)$ means higher purity of the single-photon source. Here, with $N_3 = 6000$ Hz and $t = 600$ s, $g^2(0)$ is estimated as 0.14 ± 0.04.

2.4. The Coincidence Counts of Heralded Single Photons with Switchable OAM Modes

With a proper driving voltage, the signal photons could be coupled into the OAM emitter and converted to OAM modes. When adjusting the driving voltage, the topological charge of OAM mode can be switched with the λ_s fixed at 1557.36 nm for $l = 2$–6 and 1547.72 nm for $l = -6$ to -1, respectively. Shown as the orange stars in **Figure 6**a,b, there is a linear relation between the

topological charge and driving power. Actually, the resonant order of WGM would increase with higher driving power so that the corresponding topological charge could be switched. Specifically, shown as the green squares in Figure 6a,b, for $\lambda_s = 1557.36$ nm, $l = 2$–6 is corresponding to the resonant order of 282–286, while $l = -6$ to -1 is corresponding to 306–311 for $\lambda_s = 1547.72$ nm.

To verify the generation of heralded single photons with switchable OAM modes, CCs and CAR corresponding to 11 OAM modes are measured within 10 min. As shown in Figure 6c,d, CCs of 27.5–82 and CAR of 16.33–57.63 are obtained for different OAM modes. Here, the time slot and calculation method of CAR are same as the conditions of SW-WG alone except that, for OAM modes, the final CCs and CAR are the average of those with RHCP and LHCP components. For CCs shown in Figure 6c, there is an obvious attenuation compared with SW-WG alone (CCs of 27.5–82 vs ≈77.9k within 10 min). This mainly comes from the insertion loss of OAM emitter and detection setup, which would both increase as the $|l|$ rising (see Figure S6 in Supporting Information). Hence, the CCs shown in Figure 6c goes down for $l = 2$–6 and then up for $l = -6$ to -1. For CAR shown in Figure 6d, two orange horizontal lines represent the range for SW-WG alone and most CARs of single photons with OAM states fall in this range. This indicates that the correlation between photon pairs has been kept after the modulation of OAM emitter. Moreover, these results demonstrate that the heralded single-photon source with switchable OAM modes has been successfully realized at room temperature. Benefit from the integrated scheme and crystal nature of silicon, the overall CCs and CAR have been improved significantly compared to our previous work.[29]

In our experiments, the CCs of heralded single photons with OAM modes are measured through the SPADs packaged by single mode fiber. Thus, an SLM is utilized to convert the quantum OAM modes to fundamental Gaussian mode. Since the SLM requires linear incident polarization, a quarter wave plate (QWP) and a polarizer are set in detection system to convert the polarization of generated OAM modes. Together with all these devices above and the objective lens for collection (coupling efficiency 40%), the losses in detection process are estimated to be −14.53 to −18.96 dB for different OAM modes (see Figure S6 in Supporting Information). Actually, such additional loss introduced by detection can be avoided in practical applications. It means
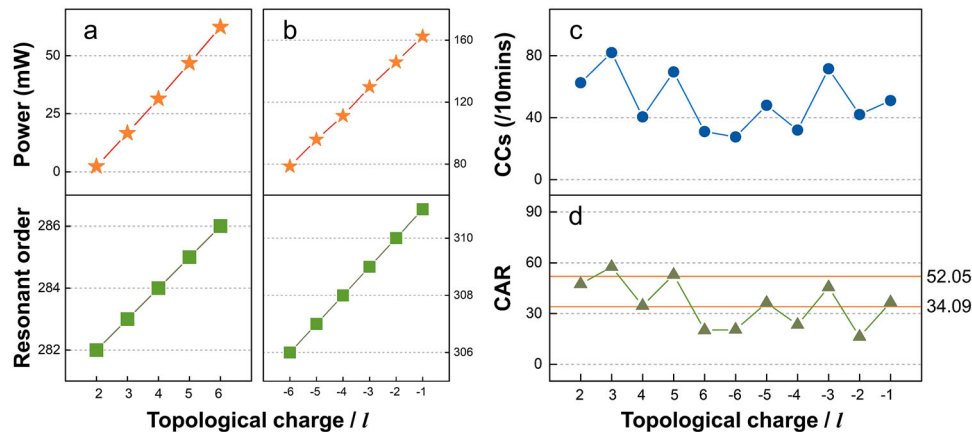
Figure 6. The characteristics of heralded single-photon source with switchable OAM modes. a,b) The driving power (orange stars) and the corresponding resonant order (green squares) versus topological charge ranging within $l = 2$–6 and $l = -6$ to -1, respectively. c) The CCs of the heralded single photons with switchable OAM modes. d) The CAR of single photons with OAM compared to that of SW-WG alone (marked as the two orange horizontal lines with values of 34.09 and 52.05, respectively).
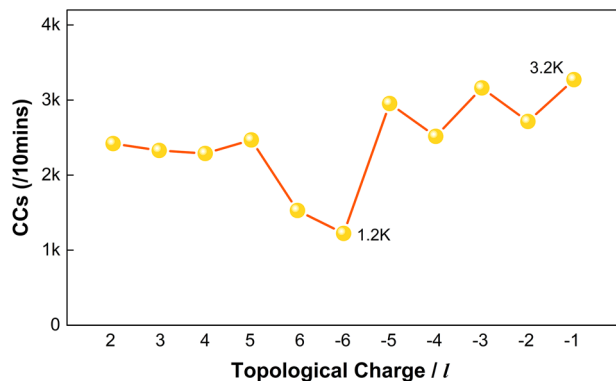
Figure 7. The estimated coincidence counts (CCs) of heralded single photons after deducting the insertion loss of detection system. The maximum and minimum values are 3.2k and 1.2k corresponding to the $l = -1$ and -6, respectively.
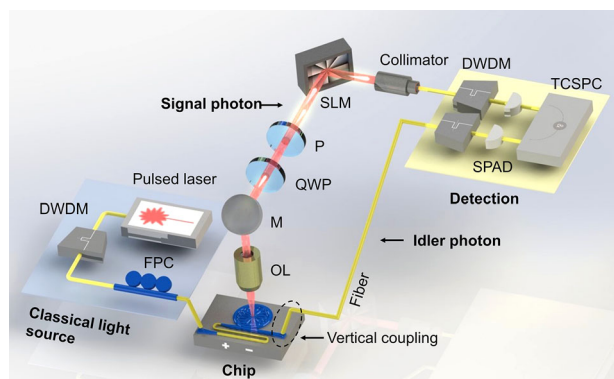
that the usable CCs of heralded single photons with OAM modes could be estimated as the value before detection setup, which is as high as 1.2k–3.2k per 10 min. The specific values corresponding to 11 OAM modes are shown in **Figure 7**. It can also be seen that the variation trend of the estimated CCs is very similar to that of the emission efficiency shown in Figure 4. Additionally, it should be mentioned that we did not directly measure the second-order correlation $g^2(\tau)$ and the indistinguishability of the whole source with OAM mode since the large detection loss makes the three-fold CCs hard to measure. Actually, the OAM emitter is a passive device and there is no significant nonlinearity in the microring cavity, we believe that the $g^2(0)$ would not be deteriorated after the OAM mode conversion and the indistinguishability can be sustained with the help of high mode purity of the OAM emitter.

3. Discussion

In this work, the whole device consists of two main units: the heralded single-photon source based on SW-WG and the integrated

OAM emitter based on SR-WG. Essentially, this is a kind of heterogenous structure assembled on a single chip to achieve both of the high nonlinear coefficient and thermo-optical coefficient. Such two characteristics are exactly beneficial to efficiently generating heralded single photons and widely switching topological charges. Actually, the same structural design could be utilized on other material platform. Particularly, the CCs can be improved by utilizing materials with higher nonlinearity and faster switching speed which can be achieved with other physical mechanism. For example, based on the lithium niobate platform, both high nonlinear coefficient[51] and high electro-optical coefficient[52] can be obtained to realize higher CCs and faster switching of topological charges. Furthermore, the spatial separation of the source and emitter provides more freedom for structural design. These two units could also be achieved based on two different materials on the same chip. The primary consideration is that the high nonlinear coefficient is essential for heralded single-photon source while low loss and feasible tunability are for OAM emitter.

Besides the photon-pair generation rate of heralded single-photon source, the emission efficiency of OAM emitter is another factor to determine the final CCs. To improve emission efficiency, both scattering grating and the coupling efficiency of download waveguides can be further optimized. For the scattering grating, the symmetrical structure is adopted in this work so that photons are scattered in both up and down directions equally while only the up-direction scattering is collected and measured in this work. Thus, if a unidirectional scattering structure or a reflective structure under the OAM emitter is utilized, the emission efficiency could increase nearly 3 dB. For the download waveguide, the coupling efficiency is considered as the same for each one. Thus, there is a trade-off between the emission efficiency and mode purity. A relatively high coupling efficiency could improve the emission efficiency, however, would lead to nonuniformity of extracted optical power from different download waveguides. Specifically, along the propagation direction within the microring cavity, the coupling power of the first download waveguide closest to the bus waveguide is the highest, and then decreases in turn. Thus, in this work, the coupling efficiency of each download

ADVANCED
SCIENCE NEWS

www.advancedsciencenews.com

LASER
& PHOTONICS
REVIEWS

www.lpr-journal.org

Figure 8. The schematic for measuring the CCs and CAR of heralded single-photon source with OAM modes. DWDM, Dense wavelength division multiplexer; FPC, fiber polarization controller; OL, objective lens; M, mirror; P, polarizer; SPAD, single photon avalanche diode; TCSPC, time-correlated single photon counting.

waveguide is set as low as 1% to avoid such nonuniformity. To increase the coupling efficiency, one possible solution is to design download waveguides with gradually varied coupling efficiency so that the extracted power can keep uniform.

4. Experimental Section

Fabrication of the Device: There were two rounds of etching corresponding to the SW-WG and SR-WG (of OAM emitter) fabricated through deep (220 nm) and shallow (70 nm) etching, respectively. Then, the titanium and aluminum were successively deposited on the top of the OAM emitter as the heat resistor and conductive electrode. The whole device was attached to a printed circuit board for voltage supply.

CCs and CAR: The experimental setup is demonstrated in **Figure 8**. After modulated to required wavelength (1552.5 nm) and polarization, the pulsed laser was coupled into the device through vertical coupling grating. When applying appropriate driving voltage, the idler photons would be scattered from output grating and detected by SPAD directly. The signal photons with OAM modes were collected by objective lens and modulated by wave plates and SLM. Considering the polarization dependence of SLM, the azimuthal polarization of OAM modes would be converted to linear polarization by a QWP and a polarizer. After converted to fundamental Gaussian mode by the phase mask on SLM, the signal photons were directed into SPAD as well. Finally, the CCs between idler and signal photons could be obtained through TCSPC. As tuning the driving voltage, the heralded single photons with different OAM modes could be generated and detected.

Supporting Information

Supporting Information is available from the Wiley Online Library or from the author.

Conflict of Interest

The authors declare no conflict of interest.

Author Contributions

X.F. and W.Z. conceived the idea and supervised the project. S.Z. designed and performed the simulations and experiments. W.Z., K.C., and F.L. provided useful discussions and comments. S.Z. and X.F. wrote the paper. Y.H. revised the manuscript. All authors approved the manuscript.

Data Availability Statement

The data that support the findings of this study are available in the Supporting Information of this article.

[1] L. Allen, M. W. Beijersbergen, R. J. C. Spreeuw, J. P. Woerdman, *Phys. Rev. A* **1992**, *45*, 8185.

[2] J. Wang, J.-Y. Yang, I. M. Fazal, N. Ahmed, Y. Yan, H. Huang, Y. Ren, Y. Yue, S. Dolinar, M. Tur, A. E. Willner, *Nat. Photonics* **2012**, *6*, 488.

[3] N. Bozinovic, Y. Yue, Y. Ren, M. Tur, P. Kristensen, H. Huang, A. E. Willner, S. Ramachandran, *Science* **2013**, *340*, 1545.

[4] M. Erhard, R. Fickler, M. Krenn, A. Zeilinger, *Light: Sci. Appl.* **2018**, *7*, 17146.

[5] Y. Yan, G. Xie, M. P. J. Lavery, H. Huang, N. Ahmed, C. Bao, Y. Ren, Y. Cao, L. Li, Z. Zhao, A. F. Molisch, M. Tur, M. J. Padgett, A. E. Willner, *Nat. Commun.* **2014**, *5*, 4876.

[6] M. Kues, C. Reimer, P. Roztocki, L. R. Cortés, S. Sciara, B. Wetzel, Y. Zhang, A. Cino, S. T. Chu, B. E. Little, D. J. Moss, L. Caspani, J. Azaña, R. Morandotti, *Nature* **2017**, *546*, 622.

[7] J. Wang, S. Paesani, Y. Ding, R. Santagati, P. Skrzypczyk, A. Salavrakos, J. Tura, R. Augusiak, L. Mančinska, D. Bacco, D. Bonneau, J. W. Silverstone, Q. Gong, A. Acín, K. Rottwitt, L. K. Oxenløwe, J. L. O'Brien, A. Laing, M. G. Thompson, *Science* **2018**, *360*, 285.

[8] M. Erhard, M. Krenn, A. Zeilinger, *Nat. Rev. Phys.* **2020**, *2*, 365.

[9] D. Cozzolino, B. Da Lio, D. Bacco, L. K. Oxenløwe, *Adv. Quantum Technol.* **2019**, *2*, 1900038.

[10] M. Mafu, A. Dudley, S. Goyal, D. Giovannini, M. McLaren, M. J. Padgett, T. Konrad, F. Petruccione, N. Lutkenhaus, A. Forbes, *Phys. Rev. A* **2013**, *8*, 032305.

[11] G. Vallone, V. D'Ambrosio, A. Sponselli, S. Slussarenko, L. Marrucci, F. Sciarrino, P. Villoresi, *Phys. Rev. Lett.* **2014**, *113*, 060503.

[12] M. Krenn, J. Handsteiner, M. Fink, R. Fickler, A. Zeilinger, *Proc. Natl. Acad. Sci. U. S. A.* **2015**, *112*, 14197.

[13] M. Zahidy, Y. Liu, D. Cozzolino, Y. Ding, T. Morioka, L. K. Oxenløwe, D. Bacco, *Nanophotonics* **2021**, *11*, 821.

[14] B. Jack, J. Leach, J. Romero, S. Franke-Arnold, M. Ritsch-Marte, S. M. Barnett, M. J. Padgett, *Phys. Rev. Lett.* **2009**, *103*, 083602.

[15] N. Uribe-Patarroyo, A. Fraine, D. S. Simon, O. Minaeva, A. V. Sergienko, *Phys. Rev. Lett.* **2013**, *110*, 043610.

[16] M. Krenn, M. Huber, R. Fickler, R. Lapkiewicz, S. Ramelow, A. Zeilinger, *Proc. Natl. Acad. Sci. U. S. A.* **2014**, *111*, 6243.

[17] J. Romero, D. Giovannini, S. Franke-Arnold, S. M. Barnett, M. J. Padgett, *Phys. Rev. A* **2012**, *86*, 012334.

[18] X. Wang, Z. Nie, Y. Liang, J. Wang, T. Li, B. Jia, *Nanophotonics* **2018**, *7*, 1533.

[19] A. Forbes, A. Dudley, M. McLaren, *Adv. Opt. Photonics* **2016**, *8*, 200.

[20] Y. Shen, X. Wang, Z. Xie, C. Min, X. Fu, Q. Liu, M. Gong, X. Yuan, *Light: Sci. Appl.* **2019**, *8*, 90.

[21] R. Fickler, R. Lapkiewicz, M. Huber, M. P. J. Lavery, M. J. Padgett, A. Zeilinger, *Nat. Commun.* **2014**, *5*, 4502.

[22] J. Leach, M. J. Padgett, S. M. Barnett, S. Franke-Arnold, J. Courtial, *Phys. Rev. Lett.* **2002**, *88*, 257901.

[23] M. P. J. Lavery, D. J. Robertson, G. C. G. Berkhout, G. D. Love, M. J. Padgett, J. Courtial, *Opt. Express* **2012**, *20*, 2110.

[24] A. Mair, A. Vaziri, G. Weihs, A. Zeilinger, *Nature* **2001**, *412*, 313.

[25] A. Vaziri, G. Weihs, A. Zeilinger, *Phys. Rev. Lett.* **2002**, *89*, 240401.

[26] T. Stav, A. Faerman, E. Maguid, D. Oren, V. Kleiner, E. Hasman, M. Segev, *Science* **2018**, *361*, 1101.

[27] R. Fickler, R. Lapkiewicz, W. N. Plick, M. Krenn, C. Schaeff, S. Ramelow, A. Zeilinger, *Science* **2012**, *338*, 640.

[28] B. Chen, Y. Wei, T. Zhao, S. Liu, R. Su, B. Yao, Y. Yu, J. Liu, X. Wang, *Nat. Nanotechnol.* **2021**, *16*, 302.

[29] S. Zhang, S. Li, X. Feng, K. Cui, F. Liu, W. Zhang, Y. Huang, *Photonics Res.* **2021**, *9*, 1865.

[30] Q. Zhou, W. Zhang, J. Cheng, Y. Huang, J. Peng, *Phys. Rev. A* **2011**, *375*, 2274.

[31] Q. Lin, G. P. Agrawal, *Opt. Lett.* **2006**, *31*, 3140.

[32] K. Harada, H. Takesue, H. Fukuda, T. Tsuchizawa, T. Watanabe, K. Yamada, Y. Tokura, S. Itabashi, *Opt. Express* **2008**, *16*, 20368.

[33] H. K. Tsang, Y. Liu, *Semicond. Sci. Technol.* **2008**, *23*, 064007.

[34] Y. Wang, P. Zhao, X. Feng, Y. Xu, K. Cui, F. Liu, W. Zhang, Y. Huang, *Sci. Rep.* **2016**, *6*, 22512.

[35] G. T. Reed, G. Mashanovich, F. Y. Gardes, D. J. Thomson, *Nat. Photonics* **2010**, *4*, 518.

[36] M. A. Foster, A. C. Turner, J. E. Sharping, B. S. Schmidt, M. Lipson, A. L. Gaeta, *Nature* **2006**, *441*, 960.

[37] J. E. Sharping, K. F. Lee, M. A. Foster, A. C. Turner, B. S. Schmidt, M. Lipson, A. L. Gaeta, P. Kumar, *Opt. Express* **2006**, *14*, 12388.

[38] X. Li, J. Chen, P. Voss, J. Sharping, P. Kumar, *Opt. Express* **2004**, *12*, 3737.

[39] H. Takesue, K. Inoue, *Opt. Express* **2005**, *13*, 7832.

[40] L. Yu, C. Yuan, R. Qi, Y. Huang, W. Zhang, *Photonics Res.* **2020**, *8*, 235.

[41] Y. Wang, X. Feng, D. Zhang, P. Zhao, X. Li, K. Cui, F. Liu, Y. Huang, *Sci. Rep.* **2015**, *5*, 10958.

[42] D. L. Andrews, M. Babiker, *The Angular Momentum of Light*, Cambridge University Press, Cambridge **2012**.

[43] C. Maurer, A. Jesacher, S. Fürhapter, S. Bernet, M. Ritsch-Marte, *New J. Phys.* **2007**, *9*, 78.

[44] R. Li, X. Feng, D. Zhang, K. Cui, F. Liu, Y. Huang, *IEEE Photonics J.* **2014**, *6*, 2200710.

[45] S. Paesani, M. Borghi, S. Signorini, A. Maïnos, L. Pavesi, A. Laing, *Nat. Commun.* **2020**, *11*, 2505.

[46] J. W. Silverstone, D. Bonneau, K. Ohira, N. Suzuki, H. Yoshida, N. Iizuka, M. Ezaki, C. M. Natarajan, M. G. Tanner, R. H. Hadfield, V. Zwiller, G. D. Marshall, J. G. Rarity, J. L. O'Brien, M. G. Thompson, *Nat. Photonics* **2014**, *8*, 104.

[47] F. Zappa, S. Tisa, A. Tosi, S. Cova, *Sens. Actuators, A* **2007**, *140*, 103.

[48] W. Becker, *Advanced Time-Correlated Single Photon Counting Techniques*, Springer Science & Business Media, Berlin/Heidelberg, Germany **2005**.

[49] H. Yu, C. Yuan, R. Zhang, Z. Zhang, H. Li, Y. Wang, Y. Wang, G. Deng, L. You, H. Song, Z. Wang, G.-C. Guo, Q. Zhou, *Photonics Res.* **2022**, *10*, 1417.

[50] Z. Ma, J.-Y. Chen, Z. Li, C. Tang, Y. M. Sua, H. Fan, Y.-P. Huang, *Phys. Rev. Lett.* **2020**, *125*, 263602.

[51] L. Arizmendi, *Phys. Status Solidi* **2004**, *201*, 253.

[52] R. S. Weis, T. K. Gaylord, *Appl. Phys. A* **1985**, *37*, 191.